Report

Cell Reports

cAMP Signals in *Drosophila* Motor Neurons Are Confined to Single Synaptic Boutons

Graphical Abstract

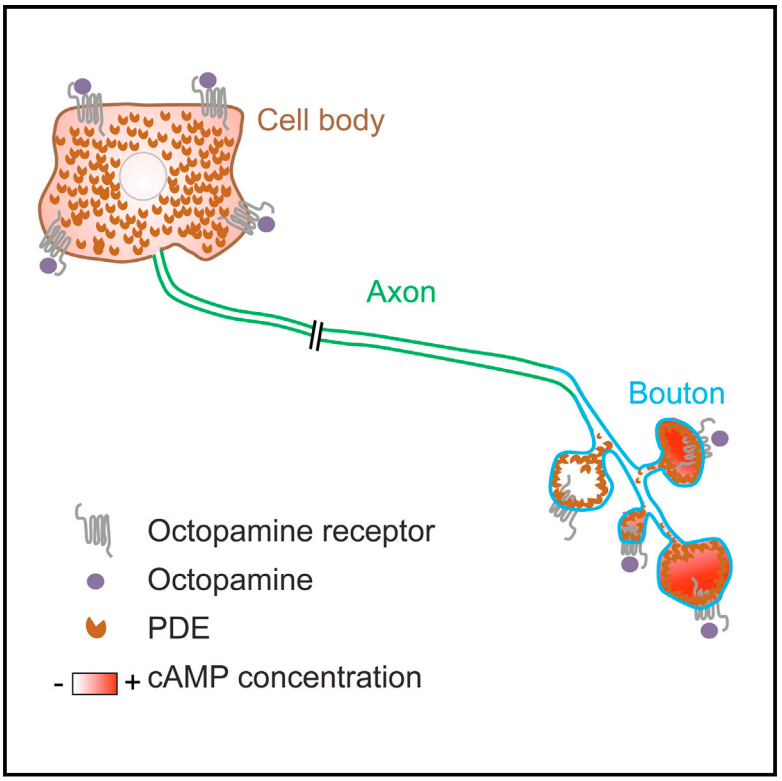

Authors

Isabella Maiellaro, Martin J. Lohse, Robert J. Kittel, Davide Calebiro

Correspondence

isabella.maiellaro@toxi.uni-wuerzburg.de (I.M.), robert.kittel@uni-wuerzburg.de (R.J.K.), davide.calebiro@toxi.uni-wuerzburg.de (D.C.)

In Brief

Maiellaro et al. find that local cAMP controls site-specific synaptic plasticity in *Drosophila* motor neurons. The expression of a genetically encoded fluorescent cAMP sensor in motor neurons allows visualization of local cAMP signals and gives insight into the formation of cAMP signaling microdomains.

Highlights

- Boutons, axon, and cell body are independent cAMP signaling compartments
- Receptors and PDEs are responsible for the compartmentalization of cAMP
- cAMP does not propagate from the bouton to the cell body
- Local cAMP increases provides a basis for site-specific control of synaptic plasticity

Maiellaro et al., 2016, Cell Reports *17*, 1238–1246
October 25, 2016
http://dx.doi.org/10.1016/j.celrep.2016.09.090

OPEN ACCESS
CellPress

Cell Reports
Report

cAMP Signals in *Drosophila* Motor Neurons Are Confined to Single Synaptic Boutons

Isabella Maiellaro,[1,4,*] Martin J. Lohse,[1,3] Robert J. Kittel,[2,*] and Davide Calebiro[1,*]
[1]Institute of Pharmacology and Toxicology and Rudolf Virchow Center, University of Würzburg, Versbacher Strasse 9, 97078 Würzburg, Germany
[2]Department of Neurophysiology, Institute of Physiology, University of Würzburg, Röntgenring 9, 97070 Würzburg, Germany
[3]Present address: Max Delbrück Center for Molecular Medicine, 13125 Berlin, Germany
[4]Lead Contact
*Correspondence: isabella.maiellaro@toxi.uni-wuerzburg.de (I.M.), robert.kittel@uni-wuerzburg.de (R.J.K.), davide.calebiro@toxi.uni-wuerzburg.de (D.C.)
http://dx.doi.org/10.1016/j.celrep.2016.09.090

SUMMARY

The second messenger cyclic AMP (cAMP) plays an important role in synaptic plasticity. Although there is evidence for local control of synaptic transmission and plasticity, it is less clear whether a similar spatial confinement of cAMP signaling exists. Here, we suggest a possible biophysical basis for the site-specific regulation of synaptic plasticity by cAMP, a highly diffusible small molecule that transforms the physiology of synapses in a local and specific manner. By exploiting the octopaminergic system of *Drosophila*, which mediates structural synaptic plasticity via a cAMP-dependent pathway, we demonstrate the existence of local cAMP signaling compartments of micrometer dimensions within single motor neurons. In addition, we provide evidence that heterogeneous octopamine receptor localization, coupled with local differences in phosphodiesterase activity, underlies the observed differences in cAMP signaling in the axon, cell body, and boutons.

INTRODUCTION

The cyclic AMP (cAMP) pathway plays fundamental roles in the nervous system, where it is prominently involved in synaptic plasticity and memory formation (Kahsai and Zars, 2011; Kandel et al., 2014). Previous studies in vertebrate and invertebrate models have shown that cAMP can propagate from dendrites to the cell body of neurons (Bacskai et al., 1993; Hempel et al., 1996), in line with the properties of a small diffusible molecule. However, a local mode of action for cAMP has also been proposed, whereby cAMP signals are localized to the periphery of neurons—namely, dendrites—creating a cAMP microdomain (Castro et al., 2010; Li et al., 2015; Neves et al., 2008; Nicol et al., 2011; Nicoll and Schmitz, 2005; Tomchik and Davis, 2009). While the existence of cAMP microdomains in neuronal dendrites is disputed based on the experimental and theoretical data (Calebiro and Maiellaro, 2014; Gervasi et al., 2010; Rich et al., 2001; Saucerman et al., 2014), very little is known about possible cAMP compartmentation in axons and how this may exert local effects at the presynaptic site. In particular, it is unclear how biochemical signals may spread from presynaptic boutons through the axon.

To investigate this question in vivo, we used the neuromuscular junction (NMJ) of *Drosophila melanogaster*, which displays different forms of synaptic plasticity (Collins and DiAntonio, 2007; Frank, 2013; Koon et al., 2011; Ljaschenko et al., 2013), many of which are dependent on cAMP signaling (Griffith and Budnik, 2006; Olsen and Keshishian, 2012). Both structural and functional properties of larval neuromuscular synapses are heterogeneous, varying between boutons belonging to the same motor neuron (Paul et al., 2015; Peled and Isacoff, 2011). How such site-specific synaptic differentiation may be achieved at high spatial resolution is currently unknown, though it is tempting to speculate that local cAMP signals play a role. Thus, the developing *Drosophila* NMJ is a powerful model to investigate the role of cAMP in synaptic plasticity under physiological conditions.

In this study, we focused on glutamatergic type Ib motor neurons (Hoang and Chiba, 2001), which are structurally regulated via G-protein-coupled receptors (GPCRs) for octopamine (Koon et al., 2011). Stimulation of these receptors has been shown to induce synaptic bouton outgrowth via a cAMP- and CREB-dependent pathway (Koon et al., 2011). Therefore, we set out to measure spatiotemporal patterns of octopamine-induced cAMP signals in these neurons. To this end, we transgenically expressed a FRET (Förster resonance energy transfer)-based sensor for cAMP (Epac1-camps; Nikolaev et al., 2004), which has previously been used to image cAMP levels in central *Drosophila* neurons (Shafer et al., 2008). Our results reveal that cAMP signals are confined to their initiation site, the individual synaptic bouton, and suggest a highly efficient local mechanism for controlling site-specific synaptic plasticity.

RESULTS

Generalized Octopamine Stimulation Induces Distinct cAMP Responses in Boutons, Axon, and Cell Body

To investigate cAMP changes in vivo and in real time upon octopamine stimulation, we expressed Epac1-camps (Nikolaev

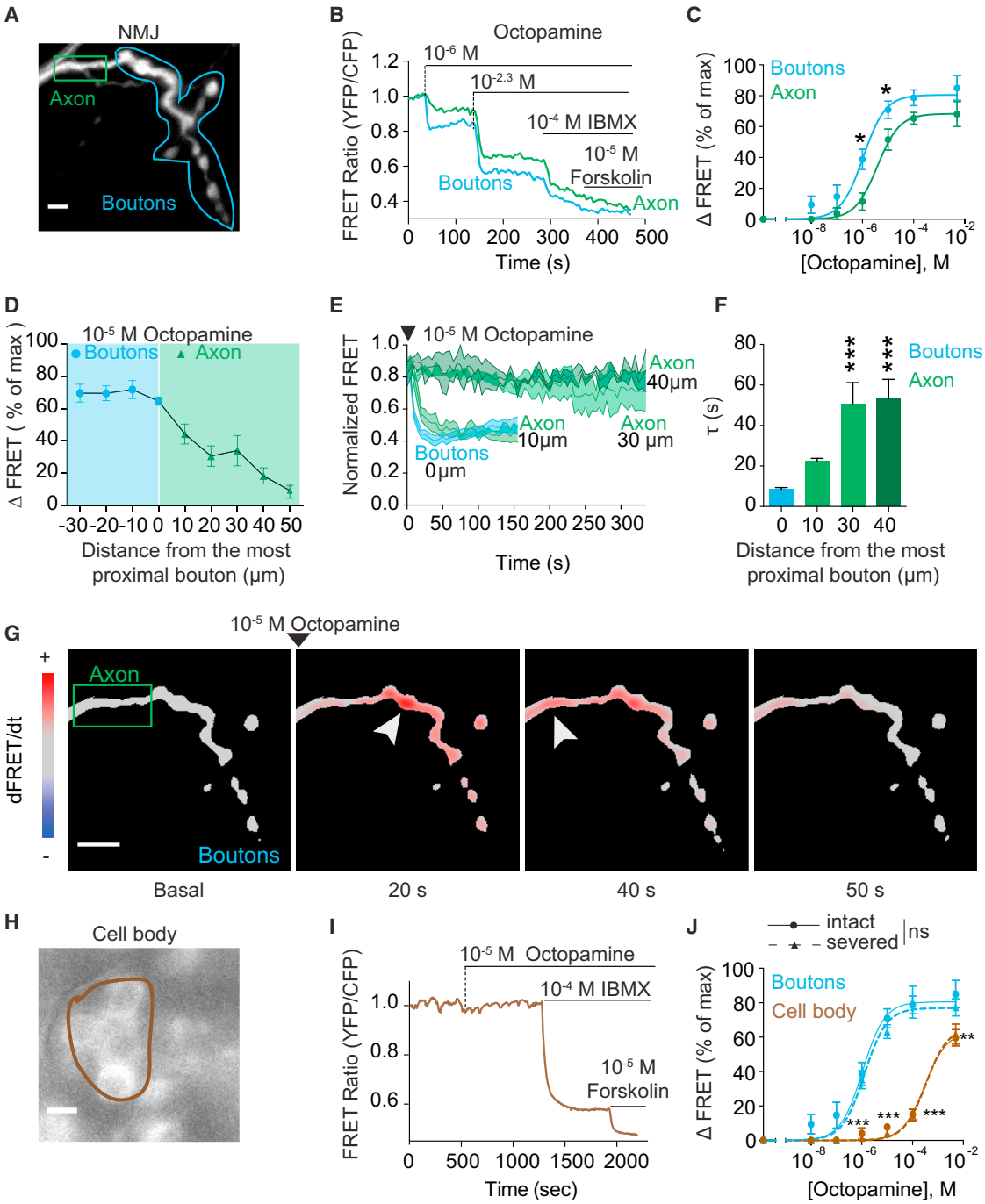

Figure 1. Dissimilar cAMP FRET Signals in Bouton, Axon, and Cell Body Induced by Generalized Octopamine Application

(A) YFP image of a *Drosophila* NMJ expressing the cAMP sensor Epac1-camps in the type Ib motor neuron innervating muscle 13.

(B) Absolute FRET ratio values recorded in the boutons and distal axon, corresponding to the regions of interest (ROIs) depicted in (A).

(C) Concentration-response curves obtained from traces like those shown in (B). ΔFRET values are expressed as percentages of the maximal response to forskolin plus IBMX and were fitted to a sigmoidal concentration-response curve.

(D) Octopamine-induced FRET changes along the motor neuron. The distances were calculated respective to the most proximal bouton (distance = 0).

(E) Time course of octopamine-induced FRET changes at NMJ. Data are normalized to the basal FRET value (set to one) and the value obtained after stimulation with forskolin and IBMX (set to zero).

(F) Time constant (τ) of FRET changes induced by stimulation with 10^{-5} M octopamine.

(G) First time-derivative analysis of cAMP changes induced by octopamine. Shown are pseudocolor images where red and blue indicate a cAMP increase or decrease, respectively. Arrowheads point to the peak response measured in the boutons (at 20 s) and in the distal axon (at 40 s).

(legend continued on next page)

et al., 2004) in third instar *Drosophila* larvae using a motor-neuron-specific promoter (Figures 1A and 1H). Live cAMP measurements were performed at type Ib glutamatergic motor neurons. The whole larvae were perfused with increasing concentrations of octopamine applied to the bath with a pipette. For normalization at the end of each experiment, the preparations were stimulated with the broad phosphodiesterase (PDE) inhibitor IBMX, followed by the direct adenylyl cyclase (AC) activator forskolin to maximally activate the Epac1-camps sensor (Figures 1B and 1I). Octopamine triggered different cAMP FRET signals in the boutons and distal axon. In particular, a 10^{-6} M concentration of octopamine produced a clear response in the boutons but only a minor effect in the distal axon, while stimulation with higher concentrations ($10^{-2.3}$ M) elicited robust cAMP responses in both compartments (Figures 1B and 1C). The potency of octopamine in eliciting cAMP FRET signals showed a 3-fold higher sensitivity in the boutons compared to the distal axon (Figure 1C). These data show that octopamine induces a gradient along the motor neuron.

Next, we aimed to understand whether cAMP FRET signals generated in the periphery of the motor neuron could reach the cell body. To this end, we analyzed the extent of the cAMP FRET signals, in space and time, evoked by 10^{-5} M octopamine, a concentration that induces structural neuronal plasticity (Koon et al., 2011). We found that, upon generalized application of octopamine, the amplitude of the cAMP response was similar in the different synaptic boutons analyzed (Figure 1D, blue region). However, in the axon, the amplitude of the cAMP response decreased nearly exponentially with distance, reaching virtually undetectable levels at ~50 μm from the most proximal bouton (Figure 1D, green region). This constitutes about 10% of the entire length of the analyzed motor neuron. Similar to the signal amplitude, the speed of the cAMP response was higher in the boutons and in the distal portion of the axon than in more proximal regions (Figures 1E and 1F).

To better illustrate the propagation of cAMP, instead of showing the direct FRET change at different time points after stimulation, we calculated the first time derivative of the FRET data. With this alternative method, the color and intensity of each pixel indicate the rate at which cAMP levels were increasing (red) or decreasing (blue) at a given time point (Figure 1G; Movie S1). The analysis clearly showed that the production of cAMP began in the boutons and only later reached a peak in the nearby portion of the axon (Figure 1G; Movie S1). Finally, we monitored the octopamine-induced cAMP FRET signals directly in the cell body localized at the level of the ventral nerve cord. Stimulation of transgenic larval preparations with a concentration of 10^{-5} M octopamine produced no detectable cAMP increases in the cell body, unless PDEs were inhibited with IBMX (Figure 1I). Moreover, the concentration-response curve showed that the cell body was 100-fold less sensitive toward octopamine than the boutons (Figure 1J). Control experiments excluded the possibility that the intracellular biosensor concentration or differences in the saturation of the sensor at rest might affect the amplitude and the kinetics of the cAMP response in the different intracellular compartments (Figures S1A–S1D). In order to determine whether cAMP FRET signals in the cell body induced by high concentrations of octopamine might be caused by cAMP generated in the bouton, we repeated the cAMP measurements in neurons with a severed axon. The resulting concentration-response curve of octopamine was indistinguishable from that obtained in intact neurons, suggesting that the cAMP in the cell body did not originate from the periphery (Figure 1J, dashed line).

Taken together, our data reveal the formation of a steep cAMP gradient upon generalized stimulation with octopamine, where cAMP FRET signals triggered in the boutons propagated only into the first portion of the axon but did not reach the cell body.

Local Stimulation Induces cAMP Signals Confined to Single Synaptic Boutons

To investigate the degree of cAMP signal compartmentalization, we performed a series of experiments in which octopamine was applied locally by means of iontophoresis (Figure 2A). The delivery of octopamine with increasing ejection currents was well within the linear range of the iontophoresis system (Figure S2A). For our experiments we chose a short stimulation (1 s) to minimize the extracellular diffusion of octopamine (Figure S2B). Such stimuli produced full activation of the receptors located on a single bouton but no equilibrium in cAMP levels (Figures 2B and 2C). Stimulation of the most distal bouton with a saturating octopamine pulse (100 nA, 1 s) resulted in a rapid and confined increase of cAMP within the targeted bouton (Figures 2C–2E), which reverted to baseline within approximately 20 s (Figures 2C and 2E). The very high sensitivity of the sensor allowed us to fully detect the physiologically relevant range in cAMP (Figures S2C–S2E), which can lead to activation of downstream targets. Remarkably, the response to such localized stimuli was confined to the stimulated bouton and spread no further than the adjacent one (Figures 2C–2E), where a minor response was seen which could be attributed to the diffusion of octopamine (Figure S2B). Overall, the cAMP gradient extended to no more than 15 μm from the stimulated bouton (Figure 2D). The time-derivative analysis of the FRET data reveals the very local increase of cAMP (indicated in red) in the stimulated bouton (Figure 2E; Movie S2), which was followed by a slower return to basal levels (indicated in blue in Figure 2E). Taken together, our results provide direct evidence that cAMP can be confined to a single synaptic bouton of a neuronal axon and that, in these circumstances, cAMP diffusion in vivo must be significantly hindered.

(H) YFP images of motor neuron cell bodies expressing the cAMP sensor.
(I) FRET traces corresponding to the ROIs depicted in (H).
(J) Concentration-response curves of intact and axon-severed larval preparations recorded in the boutons and the cell body.
Scale bars, 10 μm. Data are shown as mean ± SEM. Differences were analyzed by two-way ANOVA, followed by Bonferroni's post hoc test. *$p < 0.05$; **$p < 0.01$; ***$p < 0.001$, versus boutons; ns, statistically not significant (n = 4–8).
See also Figure S1.

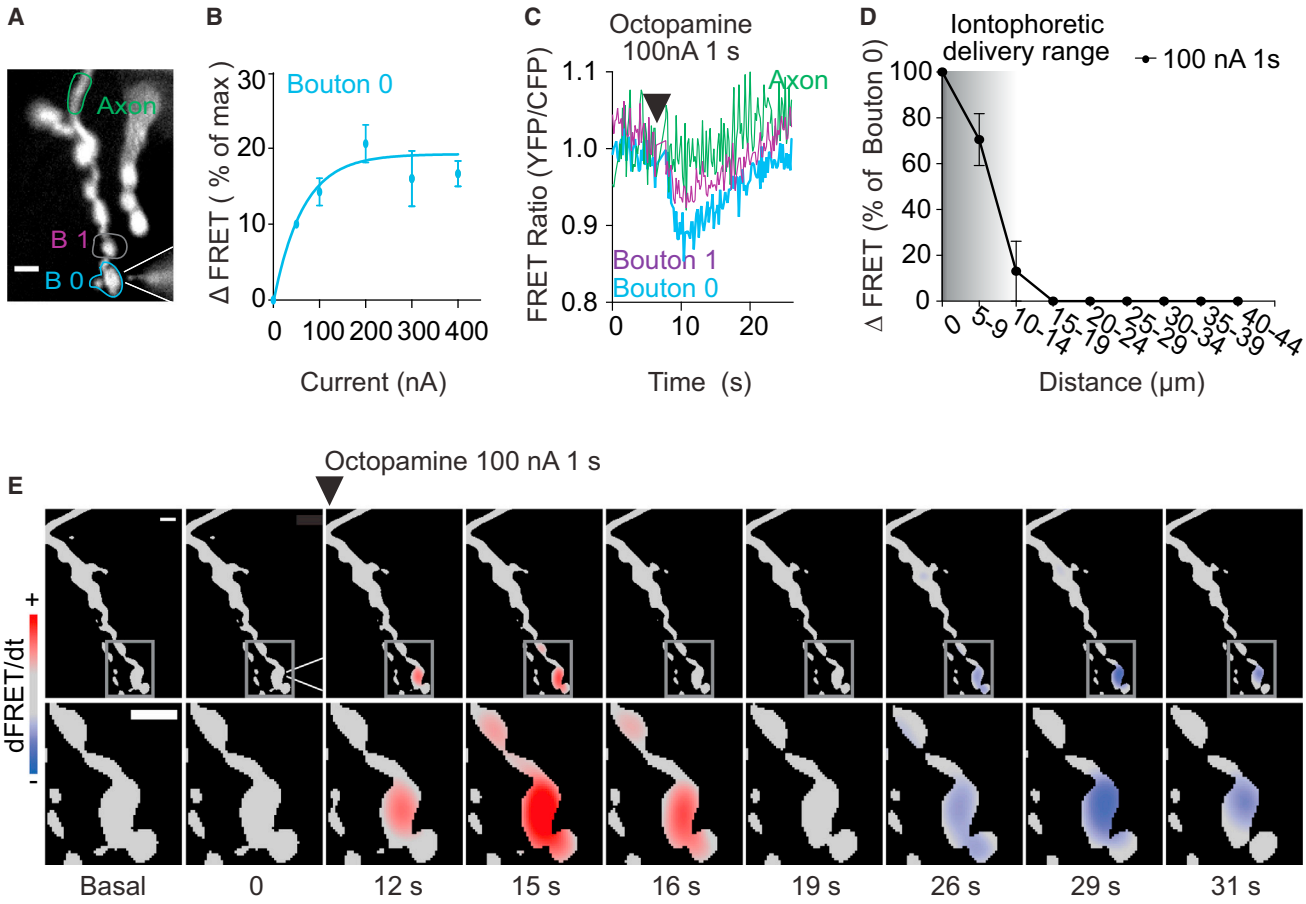

Figure 2. Iontophoretic Delivery of Octopamine to Single Boutons Elicits Confined cAMP Increases

(A) YFP image showing a glass microelectrode filled with octopamine and placed in proximity of the most distal bouton.

(B) Effect of ejection current on the cAMP FRET signals elicited in single boutons. FRET changes measured and analyzed as described in Figure 1C. ΔFRET values are plotted as a function of ejection current fitted to a monoexponential model.

(C) FRET traces obtained in the three ROIs depicted in (A), corresponding to the most distal bouton (bouton 0), the neighboring bouton (bouton 1), and the distal axon upon delivery of octopamine stimulus via the microelectrode.

(D) Spatial cAMP gradient generated by iontophoretic delivery of octopamine to bouton 0. ΔFRET values are normalized to the amplitude of the stimulated bouton and are plotted as a function of the distance from the stimulated bouton. The shaded area indicates the range of the iontophoretic delivery.

(E) First time-derivative analysis of cAMP changes induced by local octopamine delivery. Shown are pseudocolor images generated at different time points. Insets, enlarged views of the region delimited by the gray boxes. Red and blue indicate a cAMP increase or decrease, respectively.

Scale bars, 5 μm. Data are shown as mean ± SEM (n = 5–10).

See also Figure S2.

Uneven Distribution of Receptors and PDEs Contributes to cAMP Gradient Formation

The data presented earlier show that the boutons, axon, and cell body are independent cAMP signaling compartments that can, at least under certain circumstances, signal differentially. Therefore, we asked which mechanisms might contribute to isolate them.

It has been suggested that cell morphology and local differences in the surface-to-volume ratio lead to the formation of cAMP gradients between different parts of a cell, with higher cAMP concentrations in finer structures (Neves et al., 2008). In line with these arguments, we found larger cAMP FRET signals in the boutons than in the cell body (Figure 1J). However, we observed a stronger cAMP response in boutons, which have a larger diameter than the axon (~3- versus ~1 μm Ø, respectively; Figures 1B and 1D). Furthermore, we monitored a greater cAMP response in big (>2 μm Ø) than in small (<2 μm Ø) boutons (Figure 3A). This indicates that, in our system, cAMP FRET signals are potentiated in larger boutons.

We then evaluated the contribution of the proteins responsible for the formation and degradation of cAMP signals, i.e., receptors, ACs, and PDEs (Calebiro and Maiellaro, 2014). First, we assessed the contribution of octopamine receptors to the cAMP gradient induced by generalized octopamine stimulation. To do so, we monitored cAMP changes in bouton, axon, and cell body to increasing concentrations of forskolin; hence, downstream of octopamine receptors. Bypassing receptor activation led to the formation of a gradient between bouton

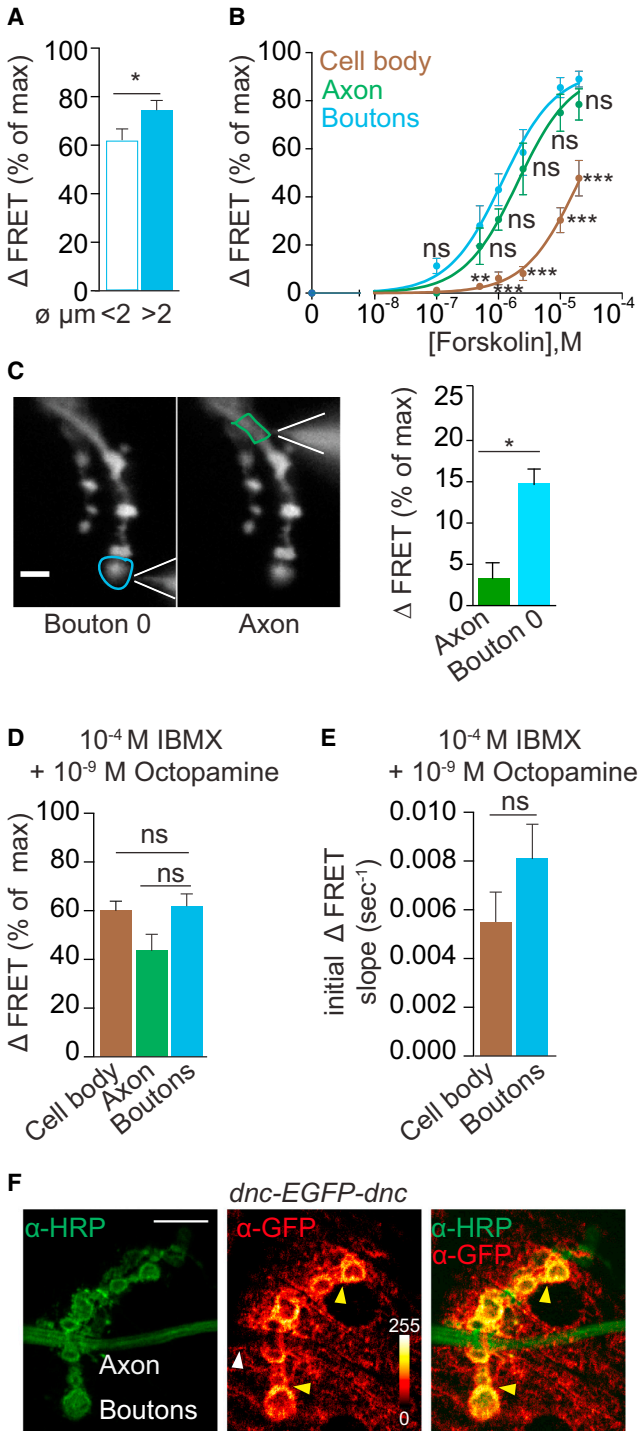

Figure 3. Differences in Functional Receptor Content and PDE Activity Explain the Octopamine-Induced cAMP Gradient

(A) Comparison of cAMP changes induced by octopamine (10^{-5} M) in boutons of different size. (n = 7). *p < 0.05 by Student's t test.

(B) Effect of direct activation of AC with forskolin. Shown are concentration-response curves recorded in the bouton, distal axon, and cell body of larvae stimulated by generalized application of increasing forskolin concentrations. ΔFRET values were calculated as described in Figure 1C. Differences were statistically significant by two-way ANOVA, followed by Bonferroni's post hoc test. **p < 0.01; ***p < 0.001 versus boutons; ns, statistically not significant (n = 4–6).

(C) Left: YFP images showing a glass microelectrode filled with octopamine and placed in close proximity to the most distal bouton 0 or the distal axon. Right: ΔFRET changes caused by iontophoretic delivery of a short octopamine stimulus (1 s, 100 nA) to the target regions. FRET values are calculated as described in Figure 1C. *p < 0.05 by Student's t test (n = 5).

(D) Amplitude of cAMP changes induced by generalized application of octopamine in the presence of the broad PDE inhibitor IBMX. ΔFRET values were calculated as described in Figure 1C. ns, statistically not significant difference by one-way ANOVA. (n = 6–10).

(E) Initial speed of cAMP accumulation induced by octopamine in the presence of IBMX. The speed was calculated by interpolating a straight line (linear regression) through the point of the normalized FRET ratio within 75 s from the stimulation with octopamine. ns, statistically non-significant difference by Student's t test. (n = 5–8).

(F) NMJ on muscle 13 of a third instar *Drosophila* larva expressing *dnc-EGFP-dnc* stained with α-HRP to mark neuronal membranes (green) and α-GFP to visualize Dnc-EGFP-Dnc (red hot). The protein was present in the boutons, reminiscent of a "fence" (yellow arrows), while absent in the axon (white arrow).

Scale bars, 10 µm. Data are shown as mean ± SEM.

See also Figures S3 and S4.

and cell body (Figure 3B) that was similar to the one seen by octopamine activation, suggesting that mechanisms other than the localization of the receptors are responsible for the differences observed between these two compartments. However, forskolin induced similar changes in bouton and axon (Figure 3B), implying that receptor localization plays a role in the octopamine-induced cAMP gradient formation between these regions. To further corroborate this hypothesis, we compared the cAMP response induced by iontophoretic delivery of octopamine to the bouton or to the axon. The axon showed virtually no local cAMP response (Figure 3C); therefore, we can infer the absence of functional octopamine receptors in this compartment.

Next, we analyzed the contribution of PDEs to the octopamine-induced cAMP gradient. Although it is undisputed that PDEs play a critical role in the dynamics of the cAMP signal, their contribution to diffusion and generation of cAMP gradients or compartments remains less clear (Conti et al., 2014). When PDE activity was blocked with IBMX in the presence of octopamine, the cAMP FRET signals were uniformly elevated along the motor neurons (Figure 3D; for comparison, see Figures 1E and 1I). The cAMP signal in the cell body was of the same magnitude as in the periphery, regardless of the applied octopamine concentration (Figure S3). Furthermore, we compared the initial rate of octopamine-induced cAMP accumulation in the presence of IBMX in the bouton versus that in the cell body as a readout of AC activity. No significant differences were observed in the rate of cAMP accumulation in the cell body and bouton, indicating that octopamine-induced AC activity was similar in the analyzed compartments (Figure 3E). Additionally, we analyzed the expression pattern of the PDEs. To achieve this, we took advantage of a newly developed *Drosophila* line in which the endogenous PDE Dunce is tagged with EGFP (*dnc-EGFP-dnc*; Nagarkar-Jaiswal et al., 2015). Staining against horseradish peroxidase (HRP) was used to visualize presynaptic arborizations, and anti-GFP staining showed the expression of the Dnc-EGFP-Dnc protein

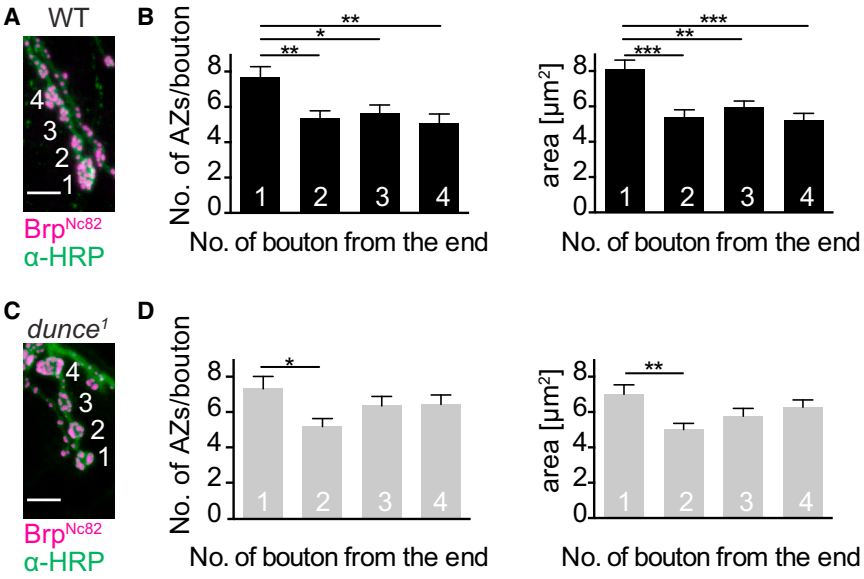

Figure 4. Impaired PDE Activity Disrupts the Structural Heterogeneity of Synaptic Boutons

(A) *Drosophila* wild-type (WT) NMJ on larval muscles 6/7 stained with α-HRP against neuronal membranes (green) and mAb Nc82 against the core active-zone (AZ) protein Bruchpilot (Brp; magenta; Wagh et al., 2006).

(B) Summary bar graphs for the number of Brp puncta (i.e., the number of AZs) per bouton and bouton area.

(C and D) *Drosophila dunce*^{1} NMJ (C) and summary bar graphs (D) as shown in (B).

Scale bars, 5 μm. Differences were statistically significant by the non-parametric Kruskal-Wallis test, followed by Dunn's multiple comparison test. $^{**}p < 0.01$; $^{***}p < 0.001$ versus bouton 1. Data are shown as mean ± SEM (n = 16).

(Figure 3F). We found that PDEs appeared largely concentrated at the plasma membrane of the synaptic boutons. Interestingly, PDEs were also localized between two neighboring boutons, reminiscent of a "fence," which could obstruct the diffusion of cAMP (Figure 3F, yellow arrows). The Dnc-EGFP-Dnc protein was undetectable in the axons (Figure 3F, white arrow), while it showed a strong signal in the cell bodies (Figure S4A). Together, these data indicate that high PDE activity contributes to a low cAMP concentration in the cell body and that the PDE distribution at the NMJ hinders cAMP diffusion from one bouton to the next.

Local cAMP Changes Contribute to Site-Specific Structural Synaptic Plasticity

At the *Drosophila* NMJ, glutamate release from motor neurons is regulated at the level of individual active zones, the specialized presynaptic sites of vesicle exocytosis (Ehmann et al., 2014; Marrus and DiAntonio, 2004; Melom et al., 2013; Peled and Isacoff, 2011; Schmid et al., 2008). Several studies have described that active-zone properties are not homogeneously distributed across motor neurons. Average ultrastructural and functional active-zone features differ between boutons (Ehmann et al., 2014; Paul et al., 2015; Peled and Isacoff, 2011) and functionally similar active zones can cluster within boutons (Melom et al., 2013). The confinement of cAMP FRET signals to a single synaptic bouton might explain how structural and functional diversity is achieved among different boutons. To test this hypothesis, we evaluated whether disturbing the cAMP metabolism could, consequently, perturb the structural gradient observed along the type Ib motor neuron on muscle 6/7. This gradient is manifested as an increase in size and active-zone number of terminal boutons compared to more proximal boutons (Paul et al., 2015). We compared wild-type (WT) and PDE mutant flies (*dunce*^{1}) (Davis and Kiger, 1981). The *dunce*^{1} mutant is a hypomorph with respect to form II PDE activity. It hydrolyzes cAMP at a significantly slower rate than the WT and should, therefore, be less efficient in segregating cAMP signals. Mutant animals show impaired learning, memory deficits, and altered motor neuron terminal growth (Zhong et al., 1992; Zhong and Wu, 2004). However, whether structural differentiation of synaptic boutons is preserved in the mutants has, to our knowledge, so far not been addressed. Indeed, in *dunce*^{1} mutants, the WT gradient in active-zone numbers per bouton was diminished, and the difference in bouton area was reduced (Figures 4A and 4B). These data demonstrate that less efficient degradation of cAMP, which will lead to a spreading out of local cAMP increases, perturbs the structural heterogeneity of synaptic boutons. Thus, these results are consistent with a site-specific control of synaptic plasticity by local cAMP.

DISCUSSION

In this study, we genetically expressed the cAMP sensor, Epac1-camps, at the *Drosophila* NMJ to monitor and quantify spatio-temporal cAMP dynamics induced by octopamine stimulation. Our results reveal an unexpectedly high degree of cAMP compartmentalization in motor neurons, which may serve as a basis for local synaptic plasticity, with cAMP FRET signals being ultimately limited to single synaptic boutons.

We identify three cAMP signaling compartments within the motor neuron: boutons, axon, and cell body. For each cellular compartment, we describe the particular mechanism responsible for the segregation of cAMP increases. Specifically, we find that boutons constitute the most reactive compartment of the motor neuron in terms of cAMP accumulation. Our results demonstrate that the production of cAMP is heterogeneous among boutons, with stronger responses to octopamine in large boutons than in smaller ones, possibly related to the increased synaptic strength measured at large boutons (Paul et al., 2015). Moreover, the activity and the specific localization of PDEs within the synaptic bouton prevent the propagation of cAMP to the cell body and its diffusion from one bouton to the next.

In contrast to the boutons, octopamine receptors seem to be absent or inaccessible in the axon, and PDEs were not detected. Accordingly, cAMP FRET signals recorded in the axon differ from those in boutons in terms of amplitude and kinetics. Hence, the axon emerges as the second independent, but not isolated, cAMP signaling compartment. Interestingly, and in contrast to dendrites (Bacskai et al., 1993; Hempel et al., 1996; Li et al., 2015), cAMP did not propagate along the axon. It remains to be clarified whether this may relate to functional differences between axons and dendrites, between species, or between specific neuron types. Finally, we determined the cell body as the third cAMP signaling compartment within the motor neuron. We show that the cell body has a very low sensitivity toward octopamine and demonstrate that cAMP FRET signals generated in the cell body are not affected by its physical isolation from the axon. High PDE activity in the cell body contributes to this local suppression of cAMP signaling and may prevent spillover activation of cAMP effectors in the cell body and in the nucleus.

Our evidence of cAMP microdomains restricted to single boutons provides a biophysical basis for the local control of synaptic plasticity. We show that spatially constrained cAMP changes help to establish differences in morphology and synaptic content of boutons, suggesting that local cAMP, bouton structure, and synapse formation are intimately linked (Ehmann et al., 2014; Paul et al., 2015; Peled and Isacoff, 2011). The observed confinement of cAMP supports the notion that individual synaptic boutons may represent largely autonomous signaling units, which can receive and integrate signals independently of the other.

The concept that cAMP could act as a local messenger was postulated almost 40 years ago (Corbin et al., 1977). The existence of cAMP microdomains has been demonstrated in other cell types (e.g., cardiomyocytes) (Zaccolo, 2011). However, in neurons, there are contradicting experimental lines of evidence and simulations concerning the existence of cAMP microdomains (Calebiro and Maiellaro, 2014). Our data clearly show that cAMP can act as a local messenger upon physiological stimulation of a neuron. The detailed spatiotemporal analysis of the dynamics of cAMP reveals that this messenger can be restricted at the micrometer level to induce highly localized physiological responses.

EXPERIMENTAL PROCEDURES

Molecular Biology and Genetics

A DNA fragment containing the whole *Epac1-camps* coding sequence flanked by an *AgeI* site at the 5′ end and a KpnI site at the 3′ end was generated by PCR amplification using *Epac1-camps* in pcDNA3 (Invitrogen) as a template and the following primers:

5′ ACATACCGGTGACACTATAGAATAGGGCC; 3′ AAGAGGGTACCAATC GAAATTAATACGACTCAC.

The amplified DNA fragment was then cloned downstream of five copies of the upstream activation sequence (UAS) in the *pJFRC7*-derived *pTL412* vector, by inserting it between the KpnI and *AgeI* sites. The obtained plasmid was sent to BestGene to generate the *20xUAS-Epac1-camps* flies by targeted germline transformation.

Fly Stocks

Flies were reared on cornmeal/agar media supplemented with yeast and kept at 25°C.

To obtain selective expression of Epac1-camps in motor neurons, we crossed flies expressing *GAL4* under the control of the *ok6* promoter (Sanyal, 2009). The *dnc-EGFP-dnc* ($y^1w^*Mi\{PT\text{-}GFSTF.2\}dnc^{MI03415\text{-}GFSTF.2}$) line was obtained from the Bloomington Drosophila Stock Center. $dunce^1$ and Canton-S stocks (Figure 4) were provided by Andreas Thum.

Semi-intact Larval NMJ Preparation

In order to expose the NMJ, third instar larvae were dissected in ice-cold calcium-free HL-3 solution (Stewart et al., 1994). The larvae were immobilized, dorsal side up, on a Sylgard 184 (Sigma-Aldrich) pad with two sharp pins. A cut was made along the dorsal midline, and after pinning down the body wall, the internal organs were carefully removed while severing the tracheal connections to the muscles. The CNS was left intact. In some experiments, the axons were severed to physically isolate the cell bodies from the NMJ. Larvae were placed in a recording chamber and imaged at room temperature in 2 mL HL-3 solution supplemented with 10 mM L-glutamate to desensitize postsynaptic receptors and thus prevent movement of the larvae. Agonists were applied in the bath with a pipette. Unless otherwise noted, the experiments were performed on type Ib motor neurons innervating muscle 13 in hemisegments A2 and A3 of male third instar larvae. Only one NMJ was analyzed per larva. Therefore, n indicates both the number of NMJs and larvae. The time constant (τ) of cAMP accumulation was calculated using a non-linear regression (monoexponential phase decay).

FRET Imaging

Ratiometric FRET imaging was performed using an upright epifluorescence microscope (Axio Observer, Zeiss) equipped with a water-immersion objective (63×/1.1 numerical aperture); a xenon lamp coupled to a monochromator (VisiView, VisiChrome); filters for CFP (436/20, 455LP dichroic) and yellow fluorescent protein (YFP; 500/20, 515LP dichroic) excitation; a beam splitter (DualView, Photometrics) with a 505LP dichroic mirror and emission filters for CFP (480/30) and YFP (535/40); and an electron-multiplied charge-coupled device (EMCCD) camera (Evolve 512, Photometrics). CFP and YFP images upon CFP excitation were captured every 5 s or every 300 ms with 80 ms of illumination time. FRET was monitored in real time with the MetaFluor 5.0 software (Molecular Devices) as the ratio between YFP and CFP emissions. The YFP emission was corrected for direct excitation of YFP at 436 nm and the bleedthrough of CFP emission into the YFP channel, as previously described (Börner et al., 2011). Images were analyzed with ImageJ software (http://rsbweb.nih.gov/ij).

Iontophoresis

Local delivery of octopamine and rhodamine was performed using a high-speed iontophoresis system with capacitance compensation (MVCS-02C, npi electronic). The headstage was mounted on a micromanipulator (NMN-21, Narishige), allowing precise positioning of the glass microelectrode. Microelectrodes were pulled with a horizontal puller (P-97, Sutter Instruments). High-resistance (70–90 MΩ) microelectrodes were filled with 10^{-5} M octopamine or rhodamine dissolved in 150 mM Na_2HPO_4 (pH 7.2), supplemented with 5% BSA. To allow visualization of the microelectrode tip during FRET imaging, the tip of the glass microelectrode was coated with Alexa Fluor 488-labeled BSA as previously described (Sasaki et al., 2012). During the experiments, larvae were continuously superfused with HL-3 solution supplemented with 10 mM glutamate in the opposite direction of the iontophoretic delivery, using a custom-made perfusion system.

Immunostaining

For the visualization of bouton structure and active zones, larvae were fixed according to Paul et al. (2015). The visualization of PDEs was performed according to Nagarkar-Jaiswal et al. (2015). Primary antibodies used were rabbit α-GFP (1:1,000; Life Technologies, #A11122) and mouse monoclonal antibody (mAb) Brp^{Nc82} (1:250; Wagh et al., 2006). Secondary antibodies used were Cy3-conjugated goat α-mouse (Invitrogen), AF488-conjugated goat α-rabbit (1:500; Life Technologies, #A11008), and Cy3- or Alexa Fluor 488-conjugated goat α-horseradish peroxidase (α-HRP) (1:250; Jackson ImmunoResearch Laboratories antibodies). Bruchpilot (Brp) puncta per bouton were quantified manually using the four terminal boutons of type Ib branches. Distal boutons were located at the end of bouton chains, whereas proximal boutons were

closer to the entry site of the motor neuron at the NMJ. The bouton area was measured via α-HRP staining. In each experiment, different genotypes were stained under the same conditions in the same vial and were analyzed by blinded observers. Confocal image stacks were obtained with a line-scanning confocal SP5 system (Leica) equipped with a 1.2 numerical aperture 63× water-immersion objective.

Statistical Analyses

Statistical analyses and curve fitting were performed with the Prism 5.0 software (GraphPad). Values are given as mean ± SEM. Differences between means were assessed by a two-tailed Student's t test (for two groups) and one- or two-way ANOVA, followed by a Bonferroni's post hoc test (for three or more groups). Differences were considered significant for values of $p < 0.05$.

SUPPLEMENTAL INFORMATION

Supplemental Information includes four figures and two movies and can be found with this article online at http://dx.doi.org/10.1016/j.celrep.2016.09.090.

AUTHOR CONTRIBUTIONS

D.C., R.J.K., and I.M. conceived the study. I.M., M.J.L., R.J.K., and D.C. designed the strategy. I.M. carried out the experiments and analyzed the data. I.M., D.C., R.J.K., and M.J.L. wrote the manuscript.

ACKNOWLEDGMENTS

The authors would like to thank Pierre Vincent and Tobias Langenhan for helpful discussions. This work was supported by grants from the German Research Foundation (DFG) to D.C. (CA 1014/1-1 and SFB/Transregio 166/C1) and R.J.K. (KI1460/1-1, SFB1047/A5, FOR2149/P3, and SFB/Transregio 166/B4) and by the Bundesministerium für Bildung und Forschung (BMBF KI 03V0830 to M.J.L.) and the European Research Council (ERC-2010-PoC 324612-FRESCA to M.J.L.).

Received: April 27, 2016
Revised: August 29, 2016
Accepted: September 27, 2016
Published: October 25, 2016

REFERENCES

Bacskai, B.J., Hochner, B., Mahaut-Smith, M., Adams, S.R., Kaang, B.K., Kandel, E.R., and Tsien, R.Y. (1993). Spatially resolved dynamics of cAMP and protein kinase A subunits in Aplysia sensory neurons. Science *260*, 222–226.

Börner, S., Schwede, F., Schlipp, A., Berisha, F., Calebiro, D., Lohse, M.J., and Nikolaev, V.O. (2011). FRET measurements of intracellular cAMP concentrations and cAMP analog permeability in intact cells. Nat. Protoc. *6*, 427–438.

Calebiro, D., and Maiellaro, I. (2014). cAMP signaling microdomains and their observation by optical methods. Front. Cell. Neurosci. *8*, 350.

Castro, L.R., Gervasi, N., Guiot, E., Cavellini, L., Nikolaev, V.O., Paupardin-Tritsch, D., and Vincent, P. (2010). Type 4 phosphodiesterase plays different integrating roles in different cellular domains in pyramidal cortical neurons. J. Neurosci. *30*, 6143–6151.

Collins, C.A., and DiAntonio, A. (2007). Synaptic development: insights from Drosophila. Curr. Opin. Neurobiol. *17*, 35–42.

Conti, M., Mika, D., and Richter, W. (2014). Cyclic AMP compartments and signaling specificity: role of cyclic nucleotide phosphodiesterases. J. Gen. Physiol. *143*, 29–38.

Corbin, J.D., Sugden, P.H., Lincoln, T.M., and Keely, S.L. (1977). Compartmentalization of adenosine 3′:5′-monophosphate and adenosine 3′:5′-monophosphate-dependent protein kinase in heart tissue. J. Biol. Chem. *252*, 3854–3861.

Davis, R.L., and Kiger, J.A., Jr. (1981). Dunce mutants of Drosophila melanogaster: mutants defective in the cyclic AMP phosphodiesterase enzyme system. J. Cell Biol. *90*, 101–107.

Ehmann, N., van de Linde, S., Alon, A., Ljaschenko, D., Keung, X.Z., Holm, T., Rings, A., DiAntonio, A., Hallermann, S., Ashery, U., et al. (2014). Quantitative super-resolution imaging of Bruchpilot distinguishes active zone states. Nat. Commun. *5*, 4650.

Frank, C.A. (2013). Homeostatic plasticity at the Drosophila neuromuscular junction. Neuropharmacology.

Gervasi, N., Tchénio, P., and Preat, T. (2010). PKA dynamics in a Drosophila learning center: coincidence detection by rutabaga adenylyl cyclase and spatial regulation by dunce phosphodiesterase. Neuron *65*, 516–529.

Griffith, L.C., and Budnik, V. (2006). Plasticity and second messengers during synapse development. Int. Rev. Neurobiol. *75*, 237–265.

Hempel, C.M., Vincent, P., Adams, S.R., Tsien, R.Y., and Selverston, A.I. (1996). Spatio-temporal dynamics of cyclic AMP signals in an intact neural circuit. Nature *384*, 166–169.

Hoang, B., and Chiba, A. (2001). Single-cell analysis of Drosophila larval neuromuscular synapses. Dev. Biol. *229*, 55–70.

Kahsai, L., and Zars, T. (2011). Learning and memory in Drosophila: behavior, genetics, and neural systems. Int. Rev. Neurobiol. *99*, 139–167.

Kandel, E.R., Dudai, Y., and Mayford, M.R. (2014). The molecular and systems biology of memory. Cell *157*, 163–186.

Koon, A.C., Ashley, J., Barria, R., DasGupta, S., Brain, R., Waddell, S., Alkema, M.J., and Budnik, V. (2011). Autoregulatory and paracrine control of synaptic and behavioral plasticity by octopaminergic signaling. Nat. Neurosci. *14*, 190–199.

Li, L., Gervasi, N., and Girault, J.A. (2015). Dendritic geometry shapes neuronal cAMP signalling to the nucleus. Nat. Commun. *6*, 6319.

Ljaschenko, D., Ehmann, N., and Kittel, R.J. (2013). Hebbian plasticity guides maturation of glutamate receptor fields in vivo. Cell Rep. *3*, 1407–1413.

Marrus, S.B., and DiAntonio, A. (2004). Preferential localization of glutamate receptors opposite sites of high presynaptic release. Curr. Biol. *14*, 924–931.

Melom, J.E., Akbergenova, Y., Gavornik, J.P., and Littleton, J.T. (2013). Spontaneous and evoked release are independently regulated at individual active zones. J. Neurosci. *33*, 17253–17263.

Nagarkar-Jaiswal, S., Lee, P.T., Campbell, M.E., Chen, K., Anguiano-Zarate, S., Gutierrez, M.C., Busby, T., Lin, W.W., He, Y., Schulze, K.L., et al. (2015). A library of MiMICs allows tagging of genes and reversible, spatial and temporal knockdown of proteins in Drosophila. eLife *4*, 4.

Neves, S.R., Tsokas, P., Sarkar, A., Grace, E.A., Rangamani, P., Taubenfeld, S.M., Alberini, C.M., Schaff, J.C., Blitzer, R.D., Moraru, I.I., and Iyengar, R. (2008). Cell shape and negative links in regulatory motifs together control spatial information flow in signaling networks. Cell *133*, 666–680.

Nicol, X., Hong, K.P., and Spitzer, N.C. (2011). Spatial and temporal second messenger codes for growth cone turning. Proc. Natl. Acad. Sci. USA *108*, 13776–13781.

Nicoll, R.A., and Schmitz, D. (2005). Synaptic plasticity at hippocampal mossy fibre synapses. Nat. Rev. Neurosci. *6*, 863–876.

Nikolaev, V.O., Bünemann, M., Hein, L., Hannawacker, A., and Lohse, M.J. (2004). Novel single chain cAMP sensors for receptor-induced signal propagation. J. Biol. Chem. *279*, 37215–37218.

Olsen, D.P., and Keshishian, H. (2012). Experimental methods for examining synaptic plasticity in Drosophila. Cold Spring Harb. Protoc. *2012*, 162–173.

Paul, M.M., Pauli, M., Ehmann, N., Hallermann, S., Sauer, M., Kittel, R.J., and Heckmann, M. (2015). Bruchpilot and Synaptotagmin collaborate to drive rapid glutamate release and active zone differentiation. Front. Cell. Neurosci. *9*, 29.

Peled, E.S., and Isacoff, E.Y. (2011). Optical quantal analysis of synaptic transmission in wild-type and rab3-mutant Drosophila motor axons. Nat. Neurosci. *14*, 519–526.

Rich, T.C., Fagan, K.A., Tse, T.E., Schaack, J., Cooper, D.M., and Karpen, J.W. (2001). A uniform extracellular stimulus triggers distinct cAMP signals in different compartments of a simple cell. Proc. Natl. Acad. Sci. USA *98*, 13049–13054.

Sanyal, S. (2009). Genomic mapping and expression patterns of C380, OK6 and D42 enhancer trap lines in the larval nervous system of Drosophila. Gene Expr. Patterns *9*, 371–380.

Sasaki, T., Matsuki, N., and Ikegaya, Y. (2012). Targeted axon-attached recording with fluorescent patch-clamp pipettes in brain slices. Nat. Protoc. *7*, 1228–1234.

Saucerman, J.J., Greenwald, E.C., and Polanowska-Grabowska, R. (2014). Mechanisms of cyclic AMP compartmentation revealed by computational models. J. Gen. Physiol. *143*, 39–48.

Schmid, A., Hallermann, S., Kittel, R.J., Khorramshahi, O., Frölich, A.M., Quentin, C., Rasse, T.M., Mertel, S., Heckmann, M., and Sigrist, S.J. (2008). Activity-dependent site-specific changes of glutamate receptor composition in vivo. Nat. Neurosci. *11*, 659–666.

Shafer, O.T., Kim, D.J., Dunbar-Yaffe, R., Nikolaev, V.O., Lohse, M.J., and Taghert, P.H. (2008). Widespread receptivity to neuropeptide PDF throughout the neuronal circadian clock network of Drosophila revealed by real-time cyclic AMP imaging. Neuron *58*, 223–237.

Stewart, B.A., Atwood, H.L., Renger, J.J., Wang, J., and Wu, C.F. (1994). Improved stability of Drosophila larval neuromuscular preparations in haemolymph-like physiological solutions. J. Comp. Physiol. A Neuroethol. Sens. Neural Behav. Physiol. *175*, 179–191.

Tomchik, S.M., and Davis, R.L. (2009). Dynamics of learning-related cAMP signaling and stimulus integration in the Drosophila olfactory pathway. Neuron *64*, 510–521.

Wagh, D.A., Rasse, T.M., Asan, E., Hofbauer, A., Schwenkert, I., Dürrbeck, H., Buchner, S., Dabauvalle, M.C., Schmidt, M., Qin, G., et al. (2006). Bruchpilot, a protein with homology to ELKS/CAST, is required for structural integrity and function of synaptic active zones in Drosophila. Neuron *49*, 833–844.

Zaccolo, M. (2011). Spatial control of cAMP signalling in health and disease. Curr. Opin. Pharmacol. *11*, 649–655.

Zhong, Y., and Wu, C.F. (2004). Neuronal activity and adenylyl cyclase in environment-dependent plasticity of axonal outgrowth in Drosophila. J. Neurosci. *24*, 1439–1445.

Zhong, Y., Budnik, V., and Wu, C.F. (1992). Synaptic plasticity in Drosophila memory and hyperexcitable mutants: role of cAMP cascade. J. Neurosci. *12*, 644–651.

Cell Reports, Volume *17*

Supplemental Information

cAMP Signals in *Drosophila* Motor Neurons Are Confined to Single Synaptic Boutons

Isabella Maiellaro, Martin J. Lohse, Robert J. Kittel, and Davide Calebiro

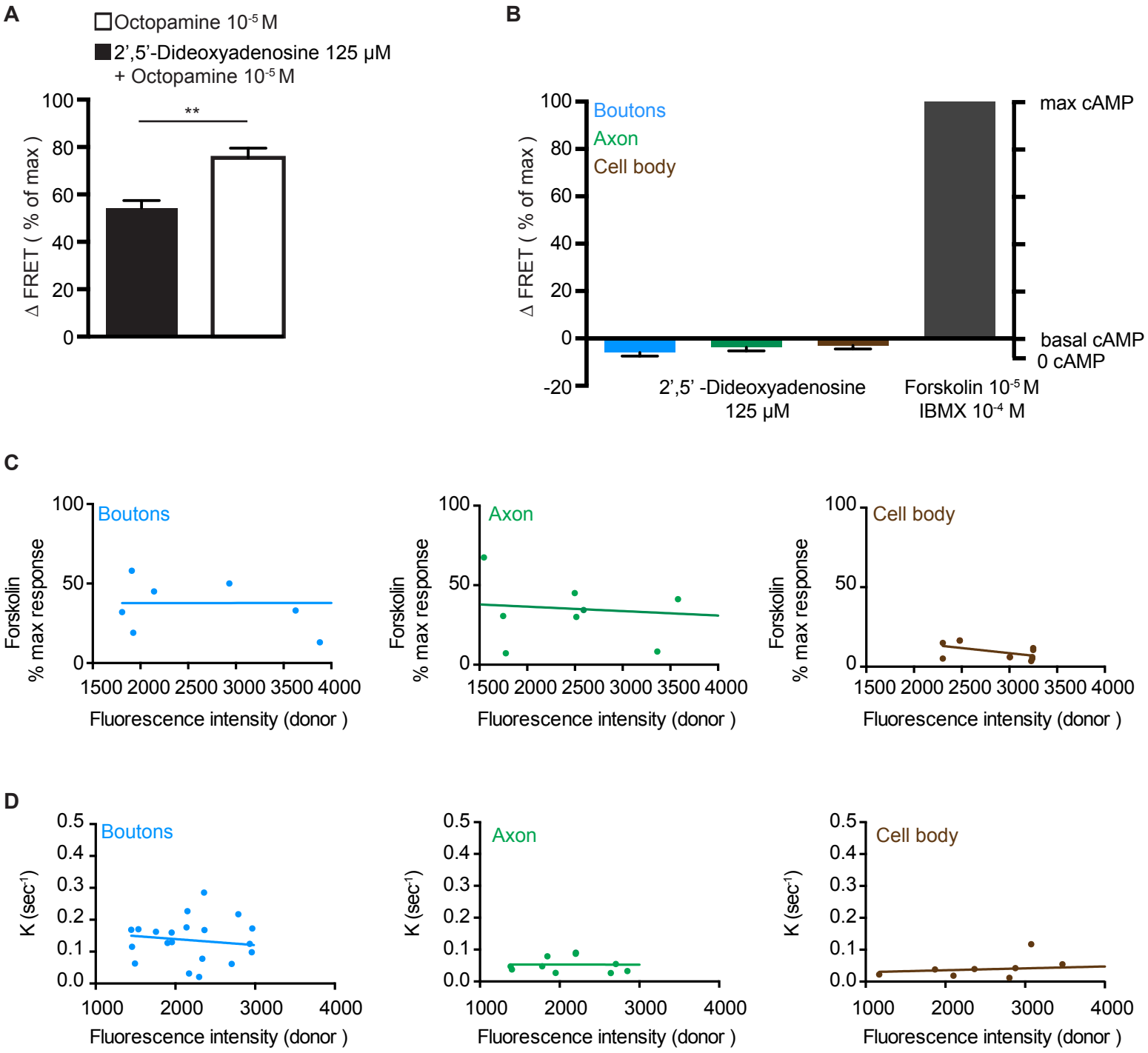

Figure S1 Related to Figure 1

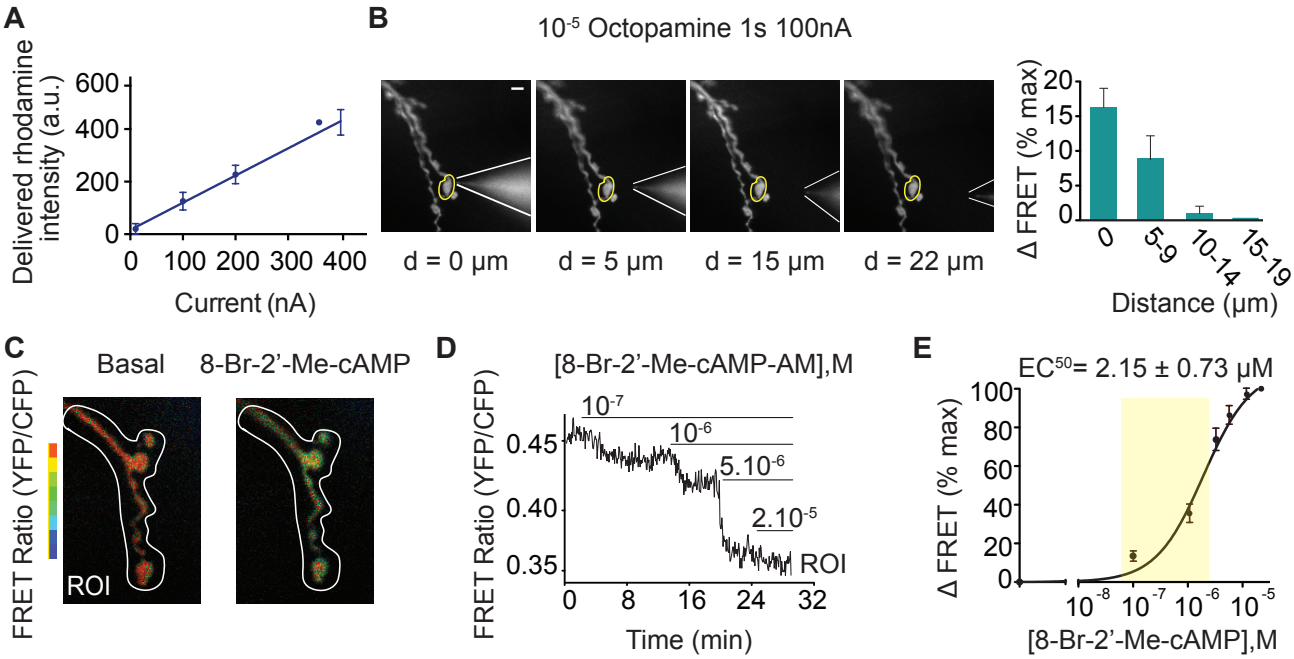

Figure S2 Related to Figure 2

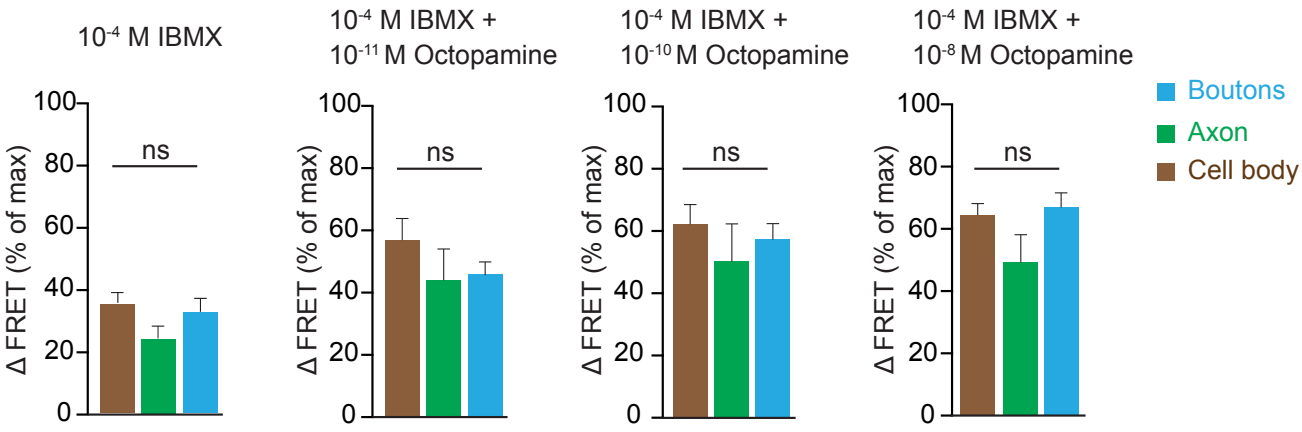

Figure S3 Related to Figure 3

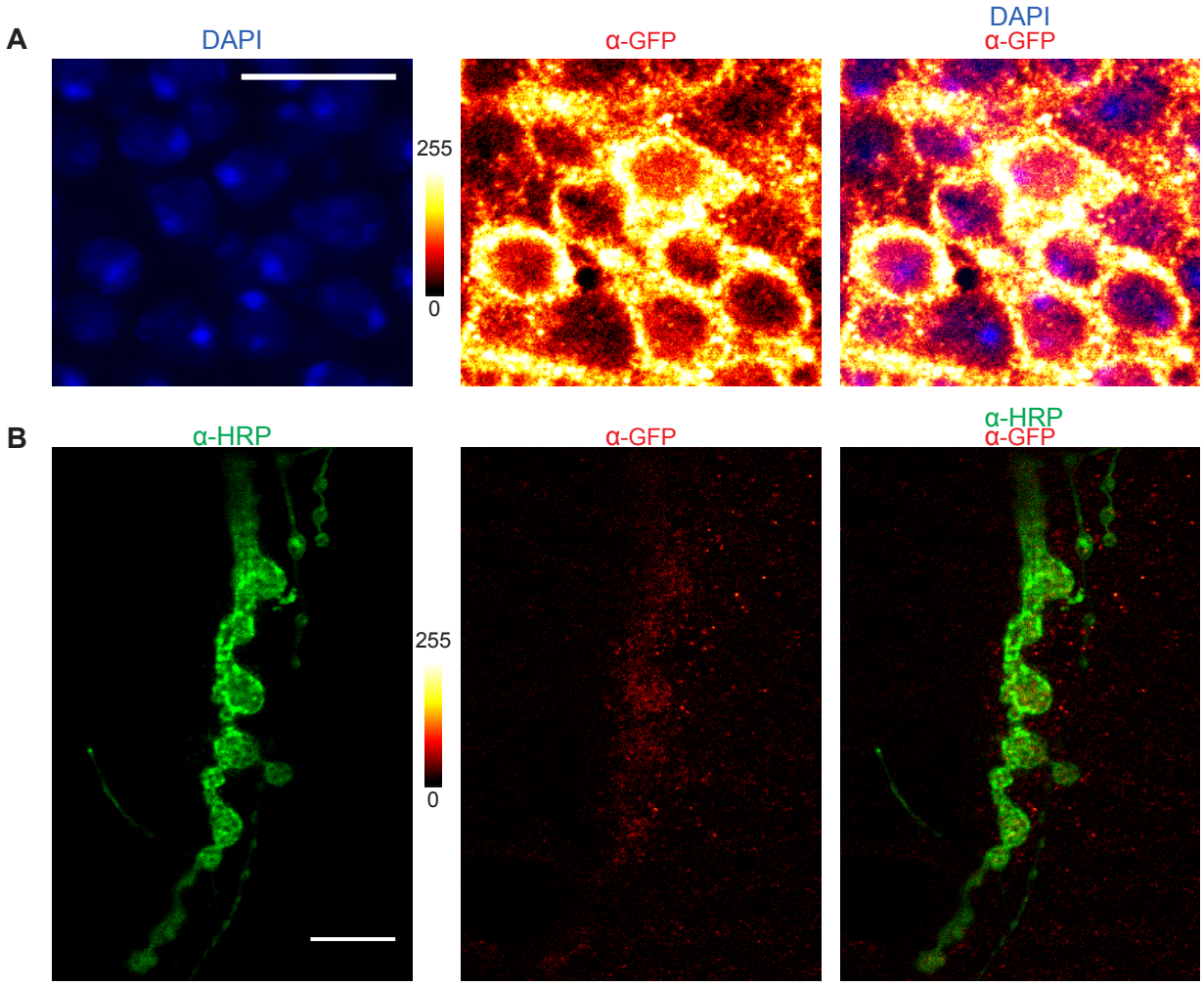

Figure S4 Related to Figure 3

Supplemental Information

Figure S1 Characterization of the transgenically expressed Epac1-camps sensor in *Drosophila* motor neurons, Related to Figure 1

(A) Efficacy of the adenylyl cyclase inhibitor 2',5'-dideoxyadenosine in *Drosophila* larvae. Motor neurons expressing the Epac1-camps sensors were preincubated with 2',5'-dideoxyadenosine and stimulated with octopamine. ΔFRET values were calculated as described in **Figure 1C**. Data are shown as mean ± s.e.m. **, P<0.01 by Student´s t-test. (n = 8).

(B) Similar basal cAMP levels in boutons, axon and cell body. *Drosophila* motor neurons were stimulated with 2',5'-dideoxyadenosine. ΔFRET values were calculated as described in **Figure 1C**. Data were not statistically different by one-way ANOVA. (n = 8).

(C) Intracellular biosensor concentration does not affect the amplitude of the cAMP response. *Drosophila* motor neurons expressing the Epac1-camps sensors were stimulated with 10^{-6} M forskolin. The amplitude of the response to forskolin was quantified in different regions of the motor neuron (boutons, axon, cell body) as a percentage of the maximal forskolin + IBMX response and plotted against fluorescence intensity. Data are shown as mean ± s.e.m. (n= 7).

(D) Intracellular biosensor concentration does not affect the kinetics of the cAMP response. *Drosophila* motor neurons were stimulated with 10^{-5} M octopamine. The rate constant K of cAMP accumulation was calculated using a non-linear regression (monoexponential phase decay) and plotted against fluorescence intensity. Data are shown as mean ± s.e.m. (n= 10-21).

Figure S2 Iontophoretic delivery of octopamine, Related to Figure 2

(A) Linearity of the iontophoretic ejection. The glass microelectrode was filled with the fluorescent dye rhodamine (10^{-5} M). The amount of dye released upon sequential pulses of 1 s with increasing ejection current was followed by fluorescence microscopy. Data fitted to a linear model. (n = 5).

(B) Range of the delivery of octopamine. Left, YFP images showing the microelectrode gradually moved away from the target bouton. Right, dependency of the FRET changes produced by a test pulse on the distance between pipette and target bouton. ΔFRET values calculated as described in **Figure 1C**. This procedure was repeated at the end of each experiment in Figure 2. (n = 10).

(C) Pseudocolor FRET images (YFP/CFP ratios) of the NMJ on muscle 13, before (basal) and after generalized stimulation with a saturating concentration (10^{-5} M) of the cell-permeable cAMP analog 8-Br-2'-Me-cAMP-AM.

(D) FRET measurement of cAMP changes induced by direct activation of the Epac1-camps sensor with increasing concentrations of 8-Br-2'-Me-cAMP-AM. Shown is a representative trace measured in the region of interest (ROI) depicted in C.
(E) Concentration-response curves obtained from traces like those shown in D, calculated as described in **Figure 1C**. Shaded yellow area represents the cAMP concentration that can activate its downstream target. Scale bar, 5 μm. Data are shown as mean ± s.e.m. (n = 8).

Figure S3 PDE inhibition abolishes the octopamine-induced cAMP gradient, Related to Figure 3
Semi-intact larval preparations were pre-incubated with the broad PDE inhibitor IBMX (10^{-4} M) and subsequently stimulated with different concentrations of octopamine. cAMP changes were monitored in boutons, the distal axon and cell body. ΔFRET values calculated as described in **Figure 1C**. ns, statistically non-significant differences by one-way ANOVA. Data are shown as mean ± s.e.m. (n = 6-10).

Figure S4 Subcellular localization of EGFP tagged PDE dunce, Related to Figure 3
(A) Third instar *Drosophila* larva expressing *dnc-EGFP-dnc* (y^1w^*Mi{PT-GFSTF.2}dnc $^{MI03415\text{-}GFSTF.2}$). Cell bodies stained with DAPI against neuronal membranes (blue) and with anti-GFP to visualize the Dnc-EGFP-Dnc expression pattern (red hot).
(B) Specificity of the α-GFP antibody. Third instar wt (Canton-S) *Drosophila* larva. NMJ on muscle 13 stained with α-HRP against neuronal membranes (green) and with α-GFP. Scale bar, 10 μm.

Movie 1 cAMP gradient at the NMJ, Related to Figure 1
First time derivative analysis of the cAMP changes induced by generalized application of octopamine (10^{-5} M). Frame interval = 5s. Scale bar, 10 μm.

Movie2 cAMP signals confined to single synaptic boutons, Related to Figure 2
First time derivative analysis of the cAMP changes induced by local stimulation of the most distal bouton with octopamine. Frame interval = 300 ms. Scale bar, 10 μm.